A unitary model for structure functions and diffractive production at small x

A. Capella, E. G. Ferreiro, C. A. Salgado
Laboratoire de Physique Théorique[*]
Université de Paris XI, Bâtiment 210, F-91405 Orsay Cedex, France

A. B. Kaidalov
ITEP, B. Cheremushkinskaya ulitsa 25
117259 Moscou, Russia

Abstract

We propose a unified approach which describes both structure functions in the small-x region and diffractive production in γ^*p-interactions. It is shown that the model, based on reggeon calculus and a quark-parton picture of the interaction, gives a good description of available experimental data in a broad region of Q^2 (including $Q^2 = 0$) with a single Pomeron of intercept $\alpha_P(0) = 1.2$. Predictions for very small x are given and the problem of saturation of parton densities is discussed.

---

[*]Unité Mixte de Recherche - CNRS - UMR n° 8627

1 Introduction

Investigation of high-energy interactions of virtual photons with nucleons and nuclei gives information on the dynamics of high-density partonic systems as well as on the transition between perturbative and nonperturbative regimes in QCD.

Experiments at HERA have found two extremely important properties of small-x physics : a fast increase of parton densities as x decreases and the existence of substantial diffractive production in deep inelastic scattering (DIS).

From a theoretical point of view there are good reasons to believe that the fast increase of the $\sigma_{\gamma^* p}$ with energy in the HERA energy range will change to a milder (logarithmic) increase at much higher energies. This is due to unitarity effects, which are related to shadowing in highly dense systems of partons - with eventual "saturation" of densities. This problem has a long history (for reviews see [1]) and has been extensively discussed in recent years [2]. It is closely connected to the problem of the dynamics of very high-energy heavy ion collisions [3].

In this paper we will address the problem of unitarization in $\gamma^* p$-interactions using the reggeon calculus [4] with a supercritical Pomeron ($\Delta_P \equiv \alpha_P(0) - 1 > 0$). In this approach the unitarization effects mentioned above are described by multi-Pomeron exchanges. The problem of the Pomeron in QCD is not solved yet. The calculation based on QCD perturbation theory leads to the so-called BFKL-Pomeron [5] and the problem of unitarization for such Pomeron has been considered by many authors [1]-[3] in the leading logarithmic approximation. However, recent calculations [6] indicate that NLO corrections are large and modify substantially the picture of high-energy interactions. In particular the intercept of the leading Regge pole depends on nonperturbative effects [6, 7].

Here, we will use a more phenomenological approach and will assume that the Pomeron is a simple pole with an intercept $\alpha_P(0) = 1.2$ determined from the analysis of high-energy hadronic interaction - when all multi-Pomeron contributions are taken into account [8].

In ref. [9] it was suggested that the increase of the effective intercept of the Pomeron, $\alpha_{eff} = 1 + \Delta_{eff}$, as Q^2 increases from zero to several GeV^2 is mostly due to a decrease of shadowing effects with increasing Q^2. A parametrization of the Q^2 dependence of Δ_{eff} such that $\Delta_{eff} \approx 0.1$ for $Q^2 \approx 0$ (as in soft hadronic interactions) and $\Delta_{eff} \approx 0.2$ (our input or bare Pomeron intercept) for Q^2 of the order of a few GeV^2, gives a good description of all existing data on $\gamma^* p$ total cross-sections in the region of $Q^2 \lesssim 5 \div 10$ GeV^2 [9, 10]. At larger Q^2, effects due to QCD evolution become important. Using the above parametrization as initial condition in the QCD evolution equation, allows to describe the data in the whole region of Q^2 studied at HERA [9, 11].

In the reggeon calculus [4] the amount of rescatterings is closely related to diffractive production. AGK-cutting rules [12] allow to calculate the cross-section of inelastic diffraction if contributions of multi-Pomeron exchanges to the elastic scattering amplitude are known. Thus, it is very important for self-consistency of theoretical models to describe not only total cross-sections, but, simultaneously, inelastic diffraction. Indeed, in the reggeon calculus the variation of Δ_{eff} with Q^2 is directly related to the corresponding variation of the ratio of diffractive to total cross-sections.

In this paper we present an explicit model which leads to the pattern of energy behaviour of $\sigma_{\gamma^* p}^{(tot)}(W^2, Q^2)$ for different Q^2 described above. Moreover, it allows to describe simultaneously diffraction production by real and virtual photons. The plan of the paper is as follows. In Section 2 the model is described. Section 3 contains the

expressions of the total cross-section $\sigma_{\gamma^*p}^{tot}$. Formulae for diffractive production are given in Section 4. Section 5 is devoted to the description of experimental data on $\sigma_{\gamma^*p}^{(tot)}(W^2, Q^2)$ and diffraction dissociation of the photon. In Section 6 we compare our results with results of other authors on this subject, discuss the problem of "saturation" and give predictions for future experiments. The parameters of the model and their numerical values are given in Appendix 1.

2 Description of the model

The amplitude of elastic γ^*p scattering at very high energy can be described in terms of the single Pomeron exchange (Fig. 1a) and multi-Pomeron exchanges (Figs. 1 b, 1c). The Pomeron exchange contribution to $\sigma_{\gamma^*p}^{tot}$ (or to the structure function $F_2 = \frac{Q^2}{4\pi^2\alpha_{e.m}}\sigma_{\gamma^*p}^{(tot)}$), increases as $\left(\frac{1}{x}\right)^\Delta$ at small $x = \frac{Q^2}{W^2+Q^2}$. The contribution of n-Pomeron exchange behaves as $\left(\frac{1}{x}\right)^{n\Delta}$. These contributions are important at very small-x to restore unitarity. A resummation of multi-Pomeron contribution is provided by Gribov reggeon calculus [4]. In this approach a two-Pomeron exchange diagram (Fig. 1b), for example, can be represented as a sum over all intermediate states (Fig. 2) which can be diffractively produced by a single Pomeron exchange. Thus the magnitude of the two Pomeron exchange in the elastic amplitude is related to the cross-section of diffractive production. The multi-Pomeron exchanges (Fig. 1c) are related by AGK-cutting rules [12] to shadowing corrections to diffractive production.

Let us first discuss the main mechanisms of diffraction dissociation of a proton and of a virtual photon. For a proton the main contribution to the diagram of Fig. 2 is due to the proton intermediate state. The dissociation of the proton will be taken into account in the quasi-eikonal approximation [13] - which works well in

hadronic interactions. As for a virtual photon, it can diffractively produce vector mesons (Fig. 3a) (the so-called quasi-elastic processes) and large mass states. For $M^2 \gg Q^2$, the latter correspond to the triple-Regge diagrams of Fig. 3b with P and f-exchanges in the t-channel. Models of this type allow to describe diffractive dissociation both at $Q^2 = 0$ [32] and at large Q^2 [14]. A simple quasi-eikonal ansatz for multi-Pomeron exchanges based on this type of model was used in ref. [15] for the description of multiparticle production in DIS. However, the quasi-eikonal approximation for diffractive dissociation of a highly virtual photon is difficult to interpret in terms of reggeon diagrams - while an explicit calculation of these diagrams for multi-Pomeron exchanges leads to too many parameters for the matrix of transition between different channels. For these reasons, we adopt here a different approach, based on the quark-parton picture of high-energy interaction of a real or virtual photon.

Taking into account that a photon dissociates into a $q\bar{q}$-pair and this pair can have multiple interactions with the target, we separate such pairs into two groups : "aligned" or asymmetric configurations, which will be denoted by A and the rest or symmetric configurations denoted by S. The A-configuration was introduced by Bjorken and Kogut [16] in the framework of the parton model in DIS and is characterized by a strongly asymmetric distribution of the relative longitudinal momenta of q and $\bar{q}$ ($z_q \ll 1$, $z_{\bar{q}} \to 1$ or viceversa). This separation into A and S components is very important at large Q^2, where the A-configuration has a large transverse size and a large interaction cross-section with the proton, while the S-component has small transverse size $(1/Q)$ and a small cross-section. On the other hand the probability of the A-configuration decreases as $1/Q^2$ and both configurations lead to the same behaviour, $\sigma_{\gamma^* p}^{(tot)} \sim 1/Q^2$, at large Q^2 [16]. What is important, however,

is that these two components give rise to a different behavior for diffraction : the A-component gives the same $1/Q^2$ behaviour for total and diffractive cross-sections, while the S-component leads to a diffractive cross-section which decreases as $(1/Q^2)^2$ at large Q^2. These results are well known and have been extensively discussed in the literature [17, 18, 19] in connection with HERA experiments.

The $q\bar{q}$-state is described, in general, by non-perturbative dynamics and only for large Q^2 and small size component it is possible to use perturbative QCD.

Finally, we stress that at present energies, due to phase space limitations, only diagrams with none or one triple reggeon interactions are important. In particular large mass diffraction corresponds to a triple Pomeron interaction diagram. However, to be more general we resum all fan-type diagrams - of the type shown in Fig. 4. This will be discussed in more detail in the next Section.

3   The total $\gamma^* p$ cross-section

We formulate the expressions of cross-sections in the impact parameter space and take into account that A- and S-components are diagonal :

$$\sigma_{\gamma^* p}^{(tot)}(s, Q^2) = 4 \int d^2b \; \sigma_{\gamma^* p}^{(tot)}(b, s, q^2) \quad , \tag{1}$$

$$\sigma_{\gamma^* p}^{(tot)}(b, s, Q^2) = \sum_i g_i(Q^2) \sigma_i^{(tot)}(b, s, Q^2) \quad i = A, S \quad . \tag{2}$$

Here $g_i(Q^2)$ is the probability of the i-th component, which according to the discussion above, has been chosen in the form

$$g_A(Q^2) = \frac{g_A(0)}{1 + \frac{Q^2}{m_A^2}} \quad ; \quad g_S(Q^2) = g_S(0) \tag{3}$$

where $g_A(0)$, and m_A^2 are considered as phenomenological free parameters.

The cross-sections $\sigma_i^{(tot)}(b, s, q^2)$ are written in the form

$$\sigma_i^{(tot)}(b, s, Q^2) = \frac{1 - \exp(-C\chi_i(b, s, Q^2)}{2C} \quad , \tag{4}$$

$$\chi_i(s, b, Q^2) = \frac{\chi_{i0}^P(s, b, Q^2)}{1 + a\chi_3(s, b, Q^2)} + \chi_{i0}^f(s, b, Q^2) \quad . \tag{5}$$

The expressions for the eikonals χ_{i0} are :

$$\chi_{i0}^k(s, b, Q^2) = C_i^k \frac{f_i(Q^2)}{\lambda_{0k}^i(Q^2, \xi)} \exp\left(\Delta_k \xi - \frac{b^2}{4\lambda_{0k}^i}\right) \tag{6}$$

with $k = P, f$ and $i = A, S$ where

$$\Delta_k = \alpha_k(0) - 1 \quad ; \quad \xi = \ln\frac{s + Q^2}{s_0 + Q^2}$$
$$\lambda_{0k}^i = R_{0ki}^2(Q^2) + \alpha_k' \, \xi \quad . \tag{7}$$

The quantity ξ is chosen in such a way as to behave as $\ln\frac{1}{x}$ for large Q^2 and as $\ln\frac{s}{s_0}$ for $Q^2 = 0$. The functions $f_i(Q^2)$ have been chosen in the form[†]

$$f_i(Q^2) = \begin{cases} \dfrac{1}{1 + Q^2/m_S^2} \quad , & i = S \\[2mm] 1 \quad , & i = A \quad . \end{cases} \tag{8}$$

The parametrization of the radius R_{0ki}^2 is given in Appendix 1. The slopes of the trajectories $\alpha_P' = 0.25$ GeV^{-2} and $\alpha_f' = 0.9$ GeV^{-2} were fixed at their values known from soft hadronic interactions.

[†]In eqs. (3) and (8) we used the simplest parametrization of $g_i(Q^2)$ and $f_i(Q^2)$ consistent with our requirements. In general $g_S(Q^2)$ and $f_A(Q^2)$ can depend on Q^2.

We turn next to the denominator in the first term of eq. (5). Here $a = g_{pp}^P(0)r_{PPP}/16\pi$ where $g_{pp}^P(0)$ and $r_{PPP}(0)$ are, respectively, the Pomeron-proton coupling and the triple Pomeron vertex, both at $t = 0$. The expression of $\chi_3(s, b, Q^2)$ is given in Section 4. Note that eqs. (4)-(6) correspond to a quasi-eikonal model [13]. For $a = 0$, its Born term, eq. (5), is a sum of Pomeron and secondary (f) reggeon exchanges. The latter is included in order to be able to use the model at energies as low as $\sqrt{s} \sim 10$ GeV. The coefficient C takes into account the dissociation of the proton and is taken to be equal to 1.5 [13]. To first order in a, the Born term, eq. (5), also contains the contribution of PPP and PfP triple regge terms (see Fig. 5). This can be easily seen by developing the first term of the r. h. s. of eq. (5) to first order in a, and using the expression of χ_3 in eqs. (26) and (27). Taken to all orders in a, eq. (5) corresponds to the resummation of all fan-type diagrams of the type shown in Fig. 4, using the Schwimmer formula [20]. Here, however, each new branching contains not only a Pomeron as in Fig. 4 but also a secondary f-reggeon exchange. These branchings are controlled by the parameters $a\gamma_P$ and $a\gamma_f$, respectively (see eq. (26))‡. As discussed in the last paragraph of Section 2, diagrams with more than one branching (i. e. more than one triple reggeon interaction) are not important at present energies due to phase space limitations.

Note that the triple Pomeron interaction introduces a large (gluonic) size component in our S-component. Actually, the separation between the two components is washed out at large Q^2 due to QCD evolution. Note also that the second term of eq. (5) (f-exchange) does not contain a denominator - as does the first one. Such a denominator would add to the f-exchange fPf and fff terms. However, such double reggeon fP and ff exchanges are already present in eq. (4) (terms $\chi_{i0}^P \chi_{i0}^f$

‡Eq. (5) is valid when these couplings are the same irrespectively of whether the branching takes place off a Pomeron or an f.

and $(\chi_{i0}^f)^2$, respectively).

In the above formulae we have neglected the real parts of the reggeon exchanges given by the signature factors. Since $\alpha_P(0)$ is not very different from unity, their effect is expected to be rather small - except when the contribution of the multi-Pomeron exchanges becomes very important. As for secondary (f) exchange, the signature factor enters only in terms with multiple f-exchange - which are not important at the comparatively high energies of the present experiments.

Many parameters of the model such as R_{0ki} are strongly constrained by the data on hadronic interactions and were fixed (see Appendix 1). Let us also note that the f exchange in $\sigma_{\gamma^*p}^{(tot)}$ is related to the valence quarks contribution, which for small x belongs to the A-component. Thus $C_S^f = 0$.

The list of all parameters and their numerical values is given in Appendix 1.

4   Diffractive production

Let us now introduce the expressions for diffraction dissociation of a virtual photon. They can be obtained, using AGK-cutting rules, from the imaginary part of the γ^*p-elastic scattering, given by eqs. (1)-(8). Neglecting s-channel iterations of the triple-Pomeron graphs, the total diffraction dissociation cross-section can be written as a sum of three components

$$\sigma_{\gamma^*p}^{(dif)} = \sum_{i=A,S} \sigma_i^{(0)} + \sigma_{PPP} \tag{9}$$

where

$$\sigma_i^{(0)} = 4g_i^2(Q^2) \int \left(\sigma_i^{(tot)}(b,s,Q^2) \right)^2 d^2b \tag{10}$$

and

$$\sigma_{PPP} = 2 \sum_i g_i^2(Q^2) \int \chi_{PPP}^i(b, s, Q^2) e^{-2C\chi_i(s,b,Q^2)} d^2b \qquad (11)$$

where $\chi_{PPP}^i(b, s, Q^2) = a\chi_i^P(s, b, Q^2)\chi_3(s, b, Q^2)$, and $\chi_i^P(s, b, Q^2)$ is given by the first term in the r. h. s. of eq. (5). For the total diffractive production cross-section, which includes the diffraction dissociation of the proton, it is necessary to multiply expressions (10), (11) by the factor $C = 1.5$, introduced in Section 3.

Note that to first order in a, σ_{PPP} corresponds to the sum of the two triple reggeon contributions in Fig. 5. Taken to all orders in a, σ_{PPP} corresponds to the resummation of all fan-type diagrams - obtained by adding to the diagrams in Fig. 5, multiple branchings with Pomeron and f-reggeon at each branching (see the discussion in Section 3). In the following, the sum of these two types of contributions will be referred to as the triple Pomeron (PPP) - although the diagram in Fig. 5b corresponds to an interference term.

With gaussian forms of the Born term in impact parameter, eq. (6), the expression (10) can be also written as follows (see second paper of [13])

$$\sigma_i^{(0)} = \frac{g_i^2(Q^2)\sigma_{B_i}}{C} \left[f\left(\frac{Z_i}{2}\right) - f(Z_i) \right] \qquad (12)$$

where

$$f(Z) = \sum_{n=1}^{\infty} \frac{(-Z)^{n-1}}{n \cdot n!} \qquad (13)$$

$$\sigma_{B_i} = 2 \int \chi_i(s, b, Q^2) d^2b \qquad (14)$$

$$Z_i = \frac{8C}{\sigma_{B_i}} \int \chi_i^2(s, b, Q^2) d^2b \quad . \tag{15}$$

In the next sections we will compare our model with differential diffractive cross-sections as functions of M^2 (square of the mass of the diffractively produced system) or of $\beta = \frac{Q^2}{M^2+Q^2}$ (which is convenient at large Q^2 and plays the same role for the Pomeron as the variable x for the proton[§]) or of the variable x_P ($x_p = \frac{x}{\beta}$). Present experiments at HERA measure the differential cross-sections integrated over the variable t (square of the momentum transfer between initial and final protons) and usually the function $F_{2D}^{(3)}$ is introduced :

$$x_P \, F_{2D}^{(3)} = \frac{Q^2}{4\pi^2\alpha_{e.m.}} \int x_P \frac{d\sigma}{dx_P dt} dt \quad . \tag{16}$$

In our model it can be written as a sum of three terms

$$F_{2D}^{(3)} = \left(\sum_i F_{2Di}^{(3)}(x, Q^2, \beta) + F_{2DPPP}^{(3)}(x, Q^2, \beta) \right) \tag{17}$$

where

$$F_{2Di}^{(3)} = F_{2Di}^{(3)B} \cdot \zeta_i \quad . \tag{18}$$

$F_{2Di}^{(3)B}(x, Q^2, \beta)$ are the lowest order (Born) approximations for these functions (their explicit forms are given below) while ζ_i are "suppression factors" due to higher order multi-Pomeron exchanges

$$\zeta_i = \left[f\left(\frac{Z_i}{2}\right) - f(Z_i) \right] \cdot \frac{8}{Z_i} \quad . \tag{19}$$

[§]It should be noted that the "structure function of the Pomeron" $F_P(\beta, Q^2)$ can be used only for the cases when multi-Pomeron exchanges are small, because in general it is impossible to separate out this amplitude.

The functions $F_{2Di}^{(3)}$ satisfy the condition

$$\int_{x_{Pmin}}^{x_{Pmax}} F_{2Di}^{(3)} dx_P = \sigma_i^{(0)}(x, Q^2) \cdot \frac{Q^2}{4\pi^2 \alpha_{e.m.}} \qquad (20)$$

where $x_{Pmin} = \frac{x}{\beta_{max}}$; $x_{Pmax} = 0.1$; $\beta_{max} = \frac{Q^2}{M_{min}^2 + Q^2}$: with $M_{min}^2 = 4m_\pi^2$.

The β-dependence of the A-component was chosen according to ref. [14], where the small-β-dependence was determined from the PPf-triple-Regge asymptotics with a simple ansatz for the behaviour at $\beta \to 1$

$$x_P F_{2DA}^{(3)B(P)}(x, Q^2, \beta) = \frac{Q^2 g_A^2(Q^2)}{4\pi^2 \alpha_{e.m.}} \int d^2 b \left(\chi_A^P(x, Q^2, b) \right)^2 \frac{\widetilde{\beta}^{2\Delta_P - \Delta_f}(1 - \beta)^{n_P(Q^2)}}{\int_{\beta_{min}}^{\beta_{max}} \frac{d\beta}{\beta} \widetilde{\beta}^{2\Delta_P - \Delta_f}(1 - \beta)^{n_P(Q^2)}} \qquad (21)$$

where $\widetilde{\beta} = \frac{Q^2 + S_0}{Q^2 + M^2} = \beta \cdot \frac{\widetilde{x}}{x}$; $\beta_{min} = \frac{x}{x_P^{max}} = 10x$. In the following all powers of $1 - \beta$ are chosen according to the arguments presented in refs. [9] and [14]:

$$n_P(Q^2) = -\frac{1}{2} + \frac{3}{2} \left(\frac{Q^2}{c + Q^2} \right) \qquad (22)$$

with $c = 3.5$ GeV^2.

The S-component should be maximal at β close to 1 and was chosen in the form

$$x_P F_{2DS}^{(3)B}(x, Q^2, \beta) = \frac{Q^2 g_S^2(Q^2)}{4\pi^2 \alpha_{e.m.}} \int d^2 b \, \chi_S^2(x, Q^2, b) \frac{\widetilde{\beta}}{\int_{\beta_{min}}^{\beta_{max}} \frac{d\beta}{\beta} \widetilde{\beta}} \qquad . \qquad (23)$$

This component contains the contribution of comparatively small masses and should decrease as $\beta \to 1$ faster than PPf contribution, eq. (21). Our choice satisfies this condition. Note that from perturbative QCD a behaviour β^3 has been found [19]. However, the contribution of this component at large Q^2, where perturbative QCD is applicable, is small ($\sim m_S^2/Q^2$). Our results are rather insensitive to the power of β in the range 1 to 3 [21].

The triple-Pomeron (PPP plus PfP) contribution $F_{2DPPP}^{(3)}(x, Q^2, \beta)$, is given by

$$x_P F_{2DPPP}^{(3)}(x, Q^2, \beta) = x_P F_{2DPPP}^{(3)B}(x, Q^2, \beta) \frac{\sigma_{PPP}}{\sigma_{PPP}^B} \quad , \tag{24}$$

where σ_{PPP} is given by eq. (11), its Born term, σ_{PPP}^B, by the same equation with $C = 0$, and

$$x_P F_{2DPPP}^{(3)B}(x, Q^2, \beta) = \frac{Q^2}{4\pi^2 \alpha_{e.m.}} 2a \int d^2b \sum_i g_i^2(Q^2) \chi_i^P(b, s, Q^2) \chi_3(s, b, Q^2, \beta) \quad , \tag{25}$$

with

$$\chi_3(s, b, Q^2, \beta) = \sum_k \gamma_k \exp\left(-\frac{b^2}{4\lambda_k\left(\frac{\widetilde{\beta}}{\widetilde{x}}\right)}\right) \left(\frac{\widetilde{\beta}}{\widetilde{x}}\right)^{\Delta_k} \frac{(1-\beta)^{n_P(Q^2)+4}}{\lambda_k\left(\frac{\widetilde{\beta}}{\widetilde{x}}\right)} \quad . \tag{26}$$

Here $\gamma_P = 1$, γ_f determines the relative strength of the PfP-contribution and $\lambda_k = R_{1k}^2 + \alpha_K' \ell n\left(\frac{\widetilde{\beta}}{\widetilde{x}}\right)$. The function $\chi_3(s, b, Q^2)$, which enters in eqs. (5) and (11) is given by

$$\chi_3(s, b, Q^2) = \int_{\beta_{min}}^{\beta_{max}} \frac{d\beta}{\beta} \chi_3(s, b, Q^2, \beta) \quad . \tag{27}$$

Since the triple Pomeron formula is not valid for low masses, we use here $M_{min} = 1$ GeV.

Note that $x_P F_{2DPPP}^{(3)B}$ is obtained from σ_{PPP}^B replacing $\chi_3(s, b, Q^2)$ by $\chi_3(s, b, Q^2, \beta)$. In this way $\int dx_P F_{2DPPP}^{(3)} dx_P = \frac{Q^2}{4\pi^2 \alpha_{e.m.}} \sigma_{PPP}$.

5   Comparison with experiment

The model outlined above was used for a joint fit of the data on the structure function $F_2(x, Q^2)$ and diffractive structure function $F_{2D}^{(3)}(x, Q^2, \beta)$ in the region of

small x ($x < 10^{-2}$) and $Q^2 \leq 10$ GeV^2[¶]. The full list of parameters and their values either fixed or obtained in the fit are given in the Appendix 1.

In Fig. 6, the dependence of $\sigma_{\gamma^* p}$ as a function of Q^2 for different energies is shown and Fig. 7 gives the x-dependence of $F_2(x, Q^2)$ for different Q^2. Our results are compared with experimental data. The description of the data is excellent. Note that the x-dependence and its variation with Q^2 is fixed in the model and is strongly correlated with the ratio of $\sigma_{\gamma^* p}^{(dif)}/\sigma_{\gamma^* p}^{(tot)}$ and its dependence on Q^2. The model confirms the Q^2-dependence of the effective intercept $\Delta_{eff} = \frac{d\ell n F_2(x, Q^2)}{d\ell n(\frac{1}{x})}$, assumed in ref. [9]. The function Δ_{eff} depends not only on Q^2, but also on x and it is shown in Fig. 8 for two different intervals of x. The function Δ_{eff} decreases as Q^2 or x decreases due to the increase of shadowing effects. It is interesting to note that, for $Q^2 = 0$, Δ_{eff} in the region of HERA energies is close to 0.13, i.e. substantially higher than in hadronic interactions. For $s \to \infty$ the cross-section $\sigma_{\gamma^* p}^{(tot)}$ has a Froissard-type behavior in $\ell n^2 \frac{s}{s_0}$.

In Figs. 9 and 10 the results of the model are compared with experimental data on diffractive structure function $F_2^{D(3)}(x, \beta, Q^2)$. The β dependence for fixed values of Q^2 and x_P is shown in Fig. 9 and the x_P-dependence for different values of Q^2 and β is presented in Fig. 10. The model reproduces the experimental data rather well. For comparison we limited ourselves to the data at low values of $x_P \leq 10^{-2}$, where the effect of the non-diffractive RRP contribution (which is not included in the model) is small. Diffractive production at $Q^2 = 0$ is reasonably well reproduced as well (Fig. 11). The dependence of diffractive cross-sections on Δ_{eff}^{dif} $\left(F_{2D}^{(3)} \sim \left(\frac{1}{x_P}\right)^{2\Delta_{eff}^{D}} \right)$ is shown in Fig. 12 as a function of Q^2 (for fixed M). The experimental points are also shown. The model predicts a weak dependence of Δ_{eff}^{dif} on Q^2 for $Q^2 > 5 \div 10$ GeV^2

[¶]Actually, for F_2 only data with $Q^2 \leq 3.5$ GeV^2 were included in the fit.

and QCD-evolution does not change this result [14].

6   Discussion and conclusions

The model we propose here for the description of total and diffractive cross-sections of interaction of a virtual photon with a proton is a natural generalization of models used for the description of high-energy hadronic interactions. The main parameter of the model - intercept of the Pomeron, $\Delta_P \equiv \alpha_P(0) - 1$, was fixed from a phenomenological study of these interactions ($\Delta_P = 0.2$) and was found to give a good description of $\gamma^* p$-interactions in a broad range of Q^2 ($0 \leq Q^2 < 10 \ GeV^2$). Note that a single Pomeron is present in the model.

It should be noticed that at higher values of Q^2, QCD evolution is important and our results should be used as initial condition in DGLAP evolution (see refs [11, 14]). In particular, due to QCD evolution, the effective Pomeron intercept in F_2 will reach values significantly larger than 1.2 at large Q^2. For diffractive process the situation is different. In this case, the effective Pomeron intercept at large Q^2 is not significantly modified as a result of QCD evolution. Moreover, the latter has rather small effect for intermediate values of β [14]. For these reasons our model, without QCD evolution, can be used here at comparatively larger values of Q^2.

Another important parameter of the theory is the triple Pomeron vertex, which appears in the parameter a. It is quite remarkable that the same value of this parameter allows to describe diffractive data both at $Q^2 = 0$ and at a few GeV^2. Thus, in our approach, the value of this parameter can be determined from soft diffraction data [22].

The variation of the photon virtuality gives a unique possibility to study unitarization effects for different scales. Let us discuss the qualitative features of our

model and its relation to the models introduced by other authors [2]. It has been mentioned above that the different role of small and large size components of a virtual photon has been emphasized by many authors [2] and perturbative calculations of unitarization effects for $\sigma_{\gamma^* p}$ have been carried out in ref. [2]. In our opinion the perturbative calculations can be valid only for the small size component (S) at large Q^2. An interesting analysis of unitarization effects for both total $\gamma^* p$-cross-section and diffractive production was performed by Golec-Biernat and Wüsthoff [2]. These authors, however, postulated an unconventional form for the elastic $\gamma^* p$-amplitude and it is not clear which diagrams lead to these unitarization effects[||]. We agree with their conclusion that for the structure function $F_2(x, Q^2)$ the unitarization effects at HERA energies are important mostly in the region of rather small $Q^2 \lesssim 2 \div 4$ GeV^2. Indeed, for $Q^2 > 2 \div 4$ GeV^2, the experimental value of Δ_{eff} is close to the one of the input (bare) Pomeron $\Delta_P = 0.2$. Within our approach this is only possible if the S-component (where unitarity corrections are higher twists) dominates. However, some unitarity corrections are present at large Q^2 due to the A-component and the triple Pomeron interaction. Moreover, they will become more important at higher energies (see the discussion in the next paragraph). However, we differ in many details from their predictions on the properties of diffractive production at large Q^2 and on the pattern of "saturation" of parton densities at large Q^2 and extremely small x.

Let us now discuss the saturation patterns in our model, i.e. the properties of $\sigma_{\gamma^* p}^{(tot)}(s, Q^2)$ in the limit $s \to \infty$. It follows from formulae (1)-(8) that for the A-

[||]Correlations in hadronic interactions have been studied for many years. It is known that they can be described [23] in an eikonal model - where the Born term, at fixed impact parameter, is used as eikonal. In the model of Golec-Biernat and Wüsthoff [2], on the contrary, the Born term is integrated over impact parameter and then eikonalized. The unitarity effects obtained in this way are very large. It is unlikely that they can describe the observed features of correlations.

component, which has a large cross-section, $\sigma_{\gamma^*p}^{(tot)}(s,b,Q^2)$ will tend to a saturation limit $1/2C$ rather fast as energy increases. On the other hand, for the small size (at large Q^2) component (S) the situation is different. If we neglect the triple-Pomeron contribution (i.e. with $a = 0$ in eq. (5)), $\chi_S(s,b,Q^2) \sim \frac{Cm_S^2}{Q^2}\exp\left(\Delta_P\xi - \frac{b^2}{4\lambda_{0P}^S}\right)$ will increase with energy until the increase of $\exp(\Delta_P\xi)$ does not overcompensate the smallness of $\frac{m_S^2}{Q^2}$. For such extremely large energies, cross-sections in the small impact parameter region will saturate to a Q^2-independent value and $F_2(x,Q^2) \sim Q^2$. This is a usual picture of saturation in perturbative QCD [1]-[3]. However, the inclusion of the PPP-fan diagrams (large distance, nonperturbative effects) according to eqs. (5), (26), (27) changes the picture drastically. In this case the increase of $\chi_3(s,b,Q^2) \sim \exp(\Delta\xi)$ will compensate the increase of $\chi_S(s,b,Q^2)$ at very large ξ and lead, at large Q^2, to a behaviour $\sigma_{\gamma^*p}^{(tot)} \sim \frac{1}{Q^2}f(\ln Q^2)$ even for $x \to 0$. (Note that for large enough Q^2 this will happen in a region where χ_S is still small).

The above effects are relatively small at present energies due to the smallness of the triple Pomeron vertex r_{PPP} which determines the constant a. However, in the "saturation limit" the properties of $\sigma_{\gamma^*p}^{(tot)}(s,Q^2)$ in our model are quite different from those in other models [2, 3]. Our predictions for $\sigma_{\gamma^*p}^{(tot)}(s,Q^2)$ for energies higher than those accessible at HERA are shown in Figs. 13.

In a forthcoming publication [21] we introduce a different but closely related model with also two components for the interaction of the $q\bar{q}$ pair : a large-size component, parametrized in the same way as the A-component in the present work, and a small-size component computed using the $q\bar{q}$ perturbative QCD wave function - with its longitudinal and transverse components. The results are very similar to the ones obtained here. Again, a single Pomeron with intercept 1.2 allows to describe

17

the data on both total $\gamma^* p$ cross-section and diffractive production.

Appendix 1

In this Appendix we give the list of all the parameters in the formulae for $\sigma_{\gamma^* p}^{(tot)}(s, Q^2)$ (or $F_2(x, Q^2)$) and diffractive production, given in sections 3 and 4 respectively - together with their numerical values. The total cross-section of $\gamma^* p$ interactions is related to the structure function F_2 as follows

$$\sigma_{\gamma^* p}^{(tot)}(s, Q^2) = \frac{4\pi^2 \alpha_{em}}{Q^2} F_2(x, Q^2) \quad , \tag{A.1}$$

where $s = W^2$ and $x = \frac{Q^2}{1 + Q^2}$. This cross-section is related by eq. (1) to the corresponding quantity, $\sigma_{\gamma^* p}^{(tot)}(b, s, Q^2)$, in the impact parameter space. The latter is written as the sum of two components (eq. (2)) with probabilities given eq. (3) where $g_A(0)$, $g_S(0)$ and m_A^2 are free parameters. Their values obtained from the fit are

$$g_A(0) = 0.15\alpha_{e.m.} \quad , \quad g_S(0) = 0.367\alpha_{e.m.} \quad , \quad m_A^2 = 0.227 \text{ GeV}^2 \quad . \tag{A.2}$$

For $a = 0$ (i.e. when triple reggeon vertices vanish ; see eq. (5)) the cross-sections $\sigma_i^{(tot)}(b, s, Q^2)$ are written in a quasi-eikonal form (eq. (4)) with Born terms given by the exchange of the Pomeron P and secondary reggeon (f) trajectories). Their expressions contain the intercepts $\alpha_k(0) = 1 + \Delta_k$ $(k = P, f)$ for which we take

$$\Delta_P = 0.2 \quad , \quad \Delta_f = -0.3 \quad . \tag{A.3}$$

They also contain five other parameters treated as free ones : C_A^P, C_S^P, C_A^f, $(C_S^f = 0)$, s_0 and m_S^2. Their values obtained in the fit are:

$$m_S^2 = 1.343 \text{ GeV}^2 \qquad , s_0 = 0.463 \text{ GeV}^2 \qquad ,$$

$$C_A^P = 0.830 \text{ GeV}^{-2} \qquad , C_S^P = 0.807 \text{ GeV}^{-2} \qquad , C_A^f = 14.28 \text{ GeV}^{-2} \quad . \qquad \text{(A.4)}$$

The value of the Pomeron intercept $\alpha_P(0) = 1.2$ has been found in soft hadronic interactions [8]. It is also consistent with the intercept of the BFKL Pomeron at NLO. When treated as a free parameter in the fit its value turns out to be very close to the one in eq. (A.3). The value of the intercept of the f has been allowed to change within some restricted limits. The value $\alpha_f(0) = 0.7$ leads to better results than the more conventional value $\alpha_f(0) = 0.5$.

Our expressions contain also the triple Pomeron term PPP whose strength is controlled by the parameter a in eq. (5), and the interference term PfP whose strength (relative to the PPP term) is given by the parameter γ_f. We use

$$a = 0.052 \text{ GeV}^{-2} \qquad \gamma_f = 8 \quad . \qquad \text{(A.5)}$$

Note that the value of a obtained in the fit agrees with the value obtained from soft diffraction (see the discussion in Section 6).

Finally we turn to the quantities

$$\lambda_{0k}^i = R_{0ki}^2(Q^2) + \alpha_k' \xi \qquad \text{(A.6)}$$

and

$$\lambda_k = R_{1k}^2 + \alpha_k' \ell n(\beta/x) \qquad \text{(A.7)}$$

in eqs. (5) and (26). They are directly related to the t-dependence of the elastic $\gamma^* p$ amplitudes and of the triple reggeon vertices, respectively, and have the standard

regge behavior as functions of ξ - or β/x. We use the conventional parameters of the reggeon slopes

$$\alpha'_P = 0.25 \text{ GeV}^{-2} \qquad , \qquad \alpha'_f = 0.9 \text{ GeV}^{-2} \quad . \tag{A.8}$$

Our results for the diffractive cross-sections integrated over t are not sensitive to the values of the parameters λ and we have fixed them to the values obtained from soft interaction data and from vector dominance. We take [24]

$$R^2_{0kA}(Q^2) = R^2_{vkA} + R^2_{pk}$$

$$R^2_{0kS}(Q^2) = \frac{R^2_{vkS}}{1 + \frac{Q^2}{m_\rho^2}} + R^2_{pk} \tag{A.9}$$

with

$$R^2_{pP} = R^2_{Pf} = 2 \text{ GeV}^{-2} \qquad , \qquad R^2_{vki} = 1 \text{ GeV}^{-2} \tag{A.10}$$

and

$$R^2_{1P} = R^2_{1f} = 2.2 \text{ GeV}^{-2} \quad . \tag{A.11}$$

Note that the Q^2-dependence of the $\gamma^*\gamma^*P$ and $\gamma^*\gamma^*f$ vertices for the S component have been chosen in such a way that the corresponding radii tend to zero for $Q^2 \to \infty$ [24].

Acknowledgments

References

[1] L. V. Gribov, E. M. Levin and M. G. Ryskin, Phys. Rep. **100**, 1 (1983).

E. Laenen and E. Levin, Ann. Rev. Nucl. Part. **44**, 199 (1994).

A. B. Kaidalov, Surveys High Energy Phys. **9**, 143 (1996).

A. H. Mueller, hep-ph/9911289.

[2] A. H. Mueller, Nucl. Phys. **B437**, 107 (1995).

A. L. Ayala, M. B. Gay Ducati and E. M. Levin, Phys. Lett. **B388**, 188 (1996) ; Nucl. Phys. **B493**, 305 (1997) ; **510**, 355 (1998).

E. Gotsman, E. Levin and U. Maor, Nucl. Phys. **B493**, 354 (1997) ; Phys. Lett. **B425**, 369 (1998) ; **B452**, 387 (1999).

E. Gotsman, E. Levin, U. Maor and E. Naftali, Nucl. Phys. **B539**, 535 (1999).

L L. Frankfurt, W. Kopf and M. Strikman, Phys. Rev. **D57**, 512 (1998) ; **D54**, 3194 (1996).

M. Mac Dermott, L. L. Frankfurt, V. Guzey and M. Strikman, hep-ph 9912547.

K. Golec-Biernat and M. Wüsthoff, Phys. Rev. **D59**, 014017 (1999) ; **D60**, 114023 (1999).

A. H. Mueller, Eur. Phys. J. **A1**, 19 (1998).

[3] L. Mc Lerran and R. Venugopalan, Phys. Rev. **D49**, 2233, 3352 (1994) ; **50**, 2225 (1994) ; **53**, 458 (1996).

J. Jalilian-Marian et al., Phys. Rev. **D59**, 014014, 034007 (1999).

A. Kovner, L. Mc Lerran and H. Weigert, Phys. Rev. **D52**, 3809, 6231 (1995).

Yu. V. Kovchegov and A. H. Mueller, Nucl. Phys. **B529**, 451 (1998).

Yu. V. Kovchegov, A. H. Mueller and S. Wallon, Nucl. Phys. **B507**, 367 (1997).

A. H. Mueller, Nucl. Phys. **B558**, 285 (1999).

A. Capella, A. Kaidalov, J. Tran Thanh Van, Heavy Ion Phys. **9**, 169 (1999).

[4] V. N. Gribov, ZhETF **57**, 654 (1967).

[5] L. N. Lipatov, Sov. J. Nucl. Phys. **23**, 338 (1976).

E. A. Kuraev, L. N. Lipatov, V.S. Fadin, Sov. Phys. JETP **45**, 199 (1977).

Y. Y. Balitsky, L. N. Lipatov, Sov. J. Nucl. Phys. **28**, 822 (1978).

[6] V. S. Fadin, L. N. Lipatov, Phys. Lett. **B429**, 127 (1998).

G. Camici, M. Ciafaloni, Phys. Lett. **B395**, 311 (1997).

[7] L. P. A. Haackman, O. V. Kancheli, J. H. Koch, Nucl. Phys. **B518**, 275 (1998).

M. Ciafaloni, D. Colferai, G. P. Salam, JHEP **9910**, 017 (1999).

[8] A. B. Kaidalov, L. A. Ponomarev and K. A. Ter-Martirosyan, Sov. J. Nucl. Phys. **44**, 468 (1986).

[9] A. Capella, A. Kaidalov, C. Merino, J. Tran Thanh Van, Phys. Lett. **B337**, 358 (1994).

[10] A. Kaidalov, C. Merino, Eur. Phys. J. **C10**, 153 (1999).

[11] A. Kaidalov, C. Merino, D. Perterman, hep-ph/9911331.

[12] V. A. Abramovsky, V. N. Gribov and O. V. Kancheli, Sov. J. Nucl. Phys. **18**, 308 (1974).

[13] K. A. Ter-Martirosyan, Nucl. Phys. **B36**, 566 (1972); Phys. Lett. **B36**, 566 (1973).

[14] A. Capella, A. Kaidalov, C. Merino, J. Tran Than Van, Phys. Lett. **B343**, 403 (1995).
A. Capella, A. Kaidalov, C. Merino, D. Perterman, J. Tran Than Van, Phys. Rev. **D53**, 2309 (1996).

[15] A. Capella, A. Kaidalov, V. Nechitailo, J. Tran Than Van, Phys. Rev. **D58**, 014002 (1998).

[16] J. D. Bjorken and J. B. Kogut, Phys. Rev. **D8**, 1341 (1973).

[17] N. N. Nikolaev and B. G. Zakharov, Zeit. Phys. **C49**, 607 (1990).

[18] L. L. Frankfurt and M. Strikman, Phys. Rep. **160**, 235 (1988).

[19] J. Bartels, J. Ellis, H. Kowalski and M. Wüsthoff, hep-ph/9803497.

[20] A. Schwimmer, Nucl. Phys. **B94**, 445 (1975).

[21] A. Capella, E. G. Ferreiro, A. B. Kaidalov and C. A. Salgado, in preparation.

[22] A. Kaidalov, Phys. Rep. **50**, 157 (1979).

[23] A. Capella and A. Krzywicki, Phys. Rev. **D18**, 4120 (1978).

[24] L. P. A. Haakman, A. Kaidalov and J. H. Kach,

[25] C. Adloff *et al* (H1 Collaboration), Nucl. Phys. **B497** (1997) 3.

[26] J. Breitweg *et al* (ZEUS Collaboration), Phys. Lett. **B407** (1997) 432.

[27] M. R. Adams *et al* (E665 Collaboration), Phys. Rev. **D54** (1996) 3006.

[28] A. Zhokin (H1 and ZEUS Collaboration), contribution to the Proceedins of the XXIX International Symposium on Multiparticle Dynamics (ISMD99), Brown University, Providence, USA, August 9-13 1999. Edited By I. Sarcevic and C.-I. Tang to be published in World Scientific.

[29] M. Derrick *et al* (ZEUS Collaboration), Z. Phys. **C72** (1996) 399; S. Aid *et al* (H1 Collaboration), Nucl. Phys. **B470** (1996) 3.

[30] C. Adloff *et al* (H1 Collaboration), Z. Phys. **C76** (1997) 613.

[31] H1 Collaboration, 29th International Conference on High-Energy Physics ICHEP98, Vancouver, Canada, July 1998.

[32] C. Adloff *et al* (H1 Collaboration), Z.Phys. C74 (1997) 221.

[33] J. Breitweg *et al* (ZEUS Collaboration), Eur. Phys. J. **C6** (1999) 43.

Figure captions

Figure 1. Single Pomeron exchange (Fig. 1a) and multi-Pomeron exchanges (Figs. 1 b, 1c).

Figure 2. Intermediate states that can be diffractively produced by a single Pomeron exchange.

Figure 3. Diagram for diffractive vector mesons production (Fig. 3a) and triple-Regge diagram (Fig. 3b) with P and f-exchanges in the t-channel (PPP and PPf).

Figure 4. Fan-type diagrams with Pomeron branchings.

Figure 5. Triple Pomeron diagrams: a) triple Pomeron PPP - already represented in Fig. 3b; b) the interference term PfP.

Figure 6. The γ^*p cross section as a function of Q^2 for different energies compared to the following experimental data: H1 1995 [25] (black points), ZEUS 1995 [26] (black squares), E665 [27] (black triangles) and ZEUSBPT97 [28] (white circles). The data at $Q^2 = 6.5$ GeV^2 (H1 1994 -black stars- and ZEUS 1994 -white stars-) are from [29].

Figure 7. F_2 as a function of x for different values of Q^2. The experimental data are the same of Fig. 6.

Figure 8. The function Δ_{eff} as a function of Q^2 for 2 intervals of x. The solid line corresponds to the interval $\widetilde{x} = \frac{Q^2+s_0}{Q^2+s} = 1.85 * 10^{-4} \div 1.16 * 10^{-5}$ and the dashed line to the interval $\widetilde{x} = 7.41 * 10^{-14} \div 4.64 * 10^{-15}$.

Figure 9. The diffractive structure function $x_P F_2^{D(3)}$ as a function of β for fixed values of Q^2 and x_P. The experimental data (H1 1994) are from [30].

Figure 10. The diffractive structure function $x_P F_2^{D(3)}$ as a function of x_P for fixed values of Q^2 and β. The experimental data (H1 1994 and H1 1995) are from [30] and [31].

Figure 11. Diffractive production at $Q^2 = 0$ GeV for two different energies. The experimental data are from [32].

Figure 12. The effective Pomeron slope Δ_{eff}^D as a function of Q^2 for $M_X = 5$ GeV. The experimental values are from ZEUS 1994 [33].

Figure 13. Our predictions for the $\gamma^* p$ cross section at energies higher than those accessible at HERA. The experimental data are the same as in Figs. 6 and 7.
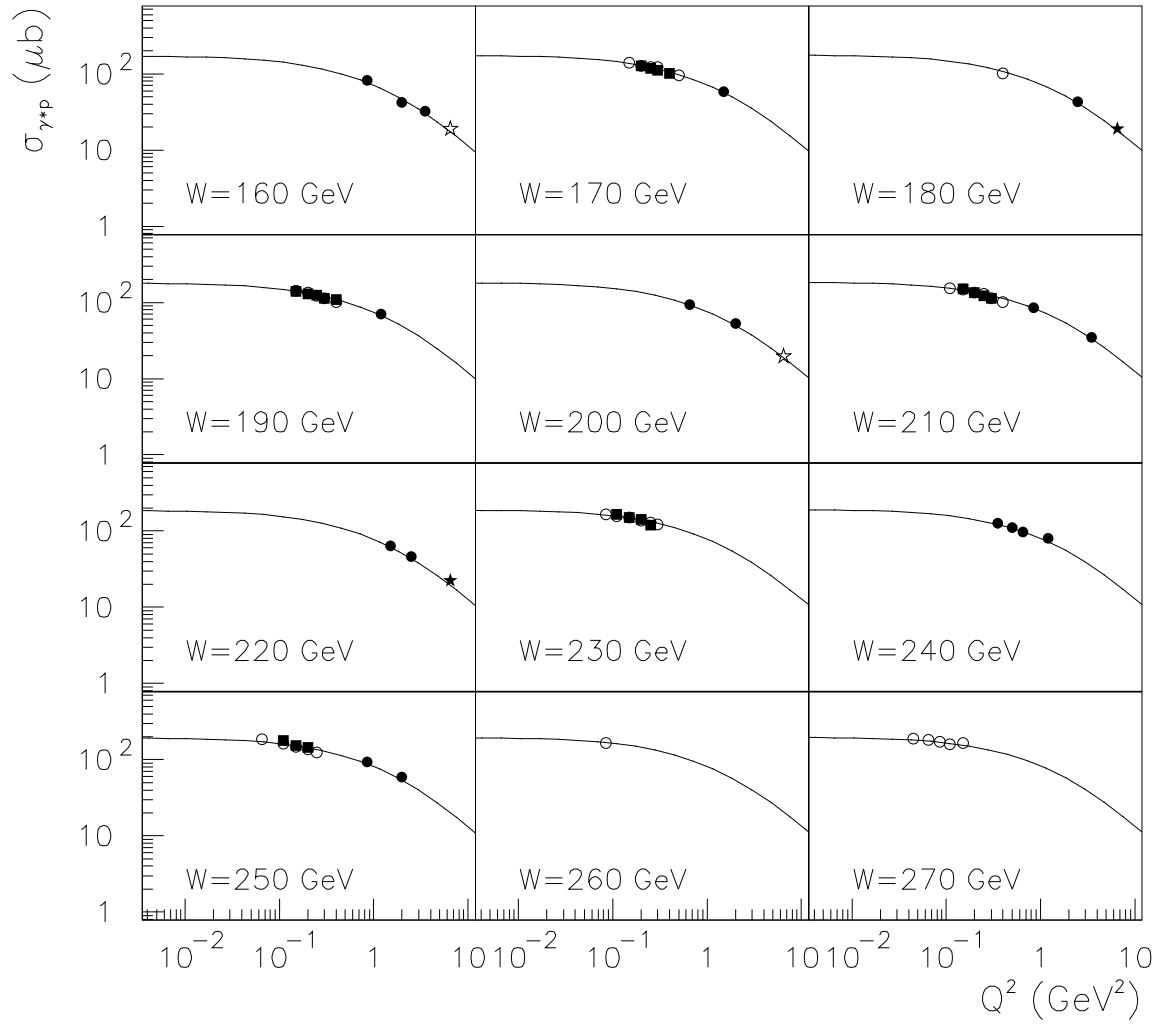
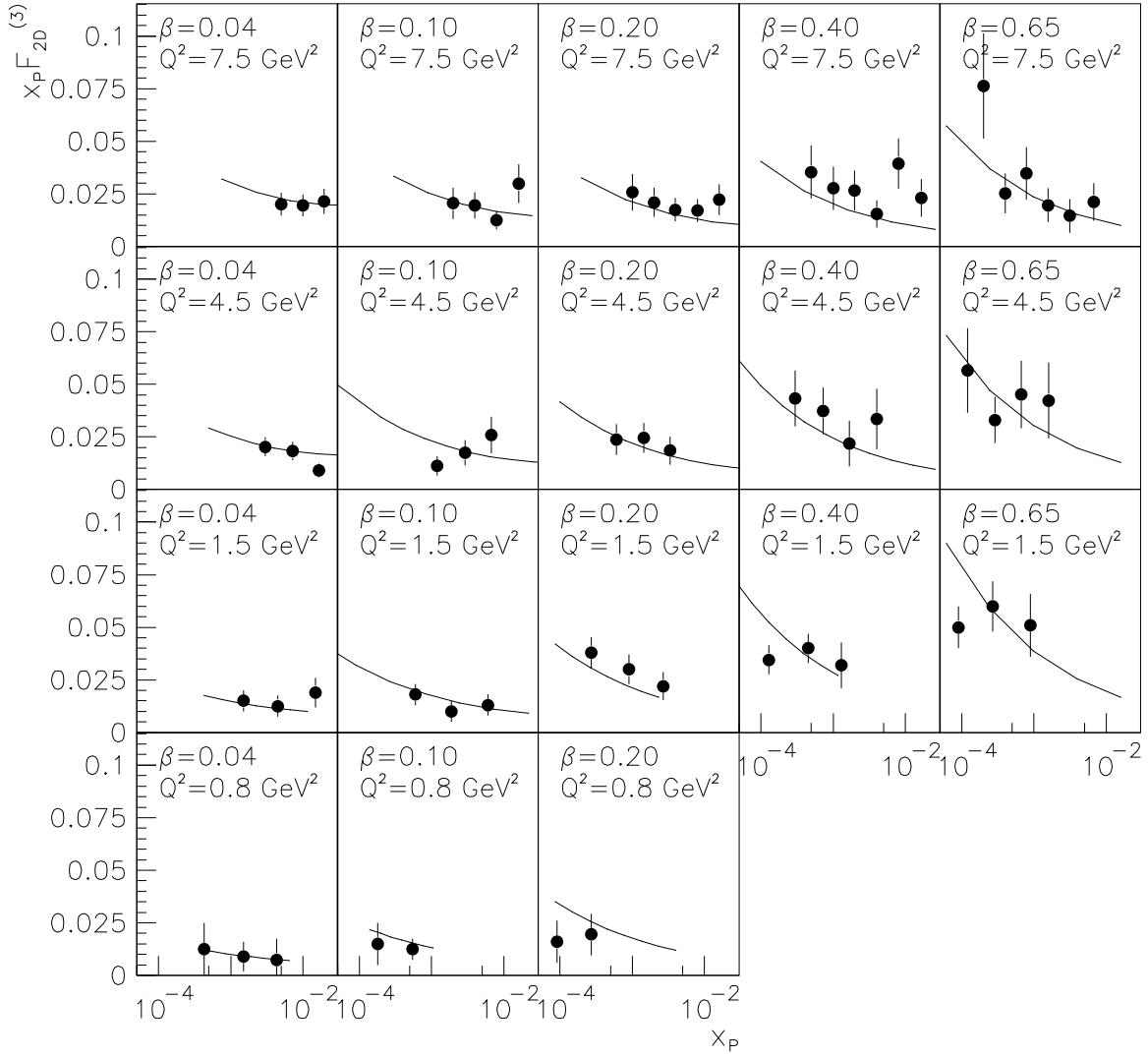**Figure 1**

Figure 2

Figure 3

a)

b)
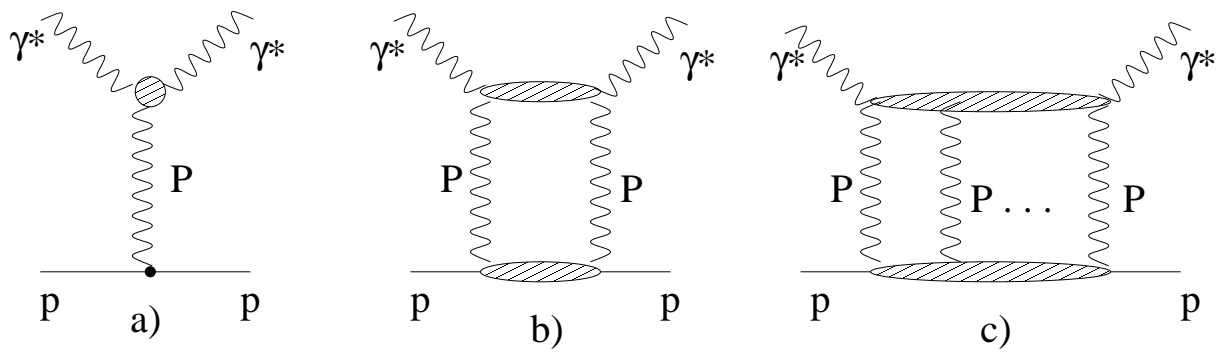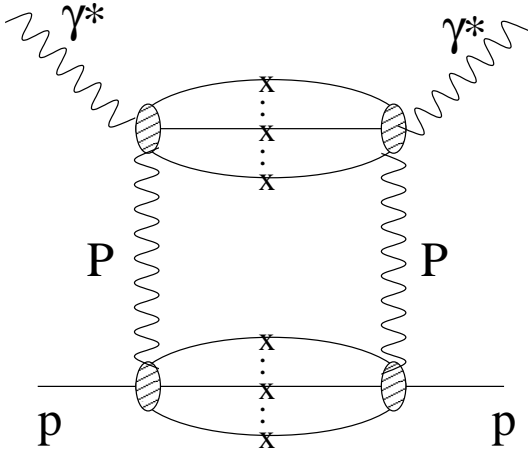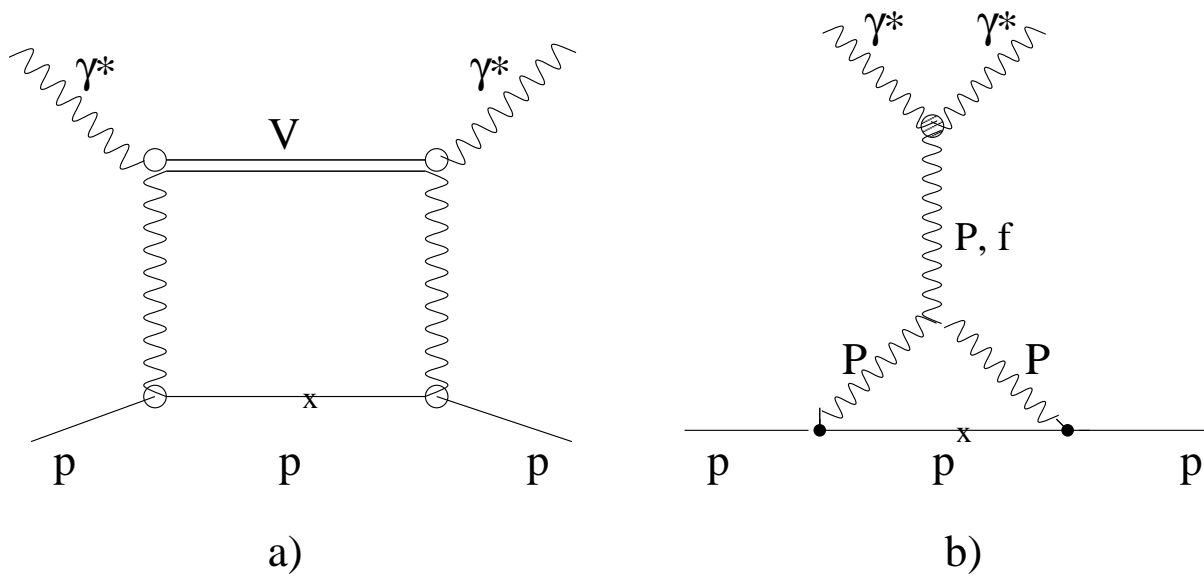
Figure 4

Figure 5

a)   b)

Figure 6

σ_{γ*p} (μb) vs Q² (GeV²) — multi-panel plots labeled W=160 GeV, W=170 GeV, W=180 GeV, W=190 GeV, W=200 GeV, W=210 GeV, W=220 GeV, W=230 GeV, W=240 GeV, W=250 GeV, W=260 GeV, W=270 GeV

Figure 7

F_2

Q^2=0.80 GeV^2

Q^2=0.85 GeV^2

Q^2=1.20 GeV^2

Q^2=1.50 GeV^2

Q^2=2.00 GeV^2

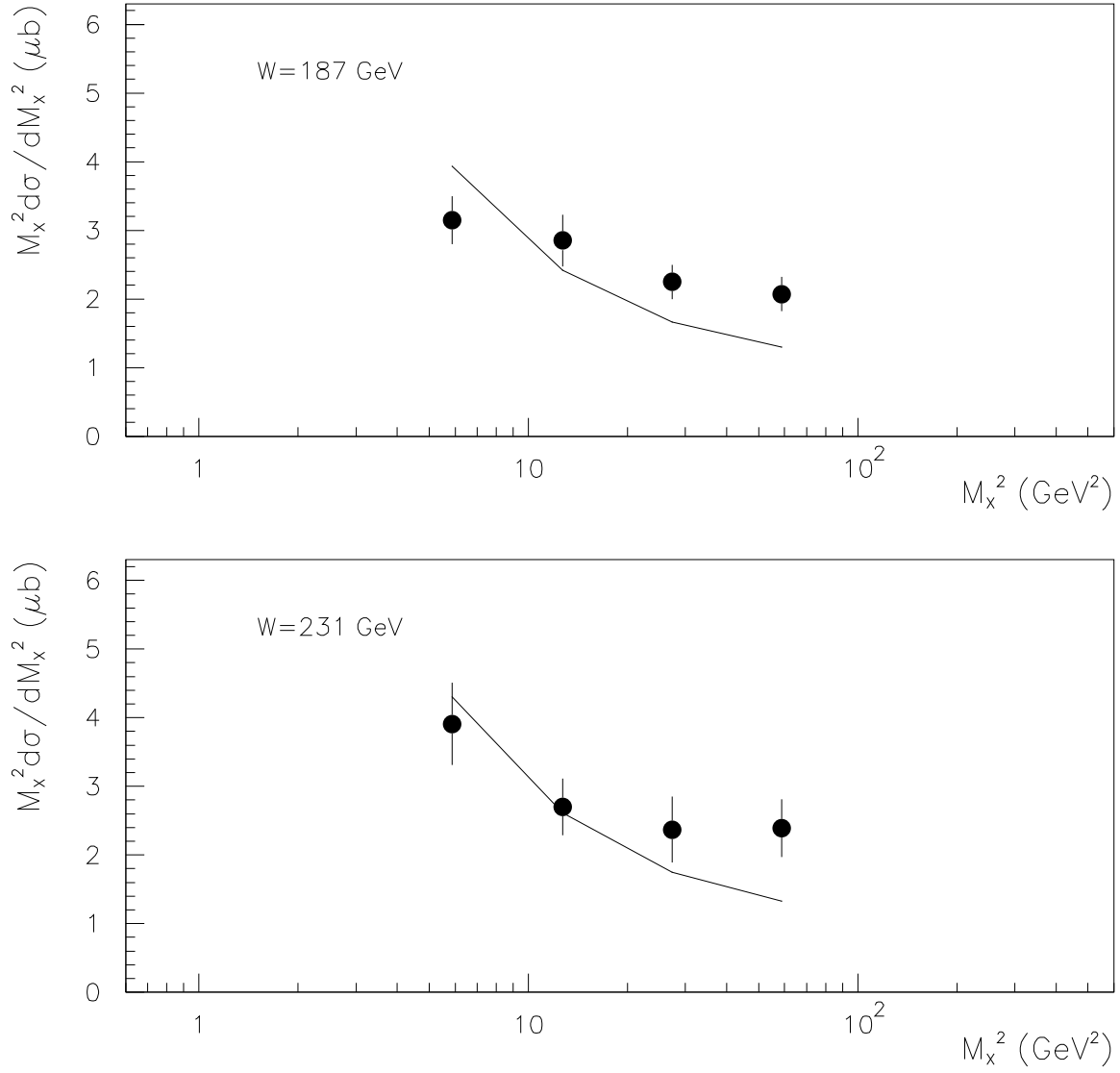Q^2=2.50 GeV^2

Q^2=3.50 GeV^2

Q^2=6.50 GeV^2

X
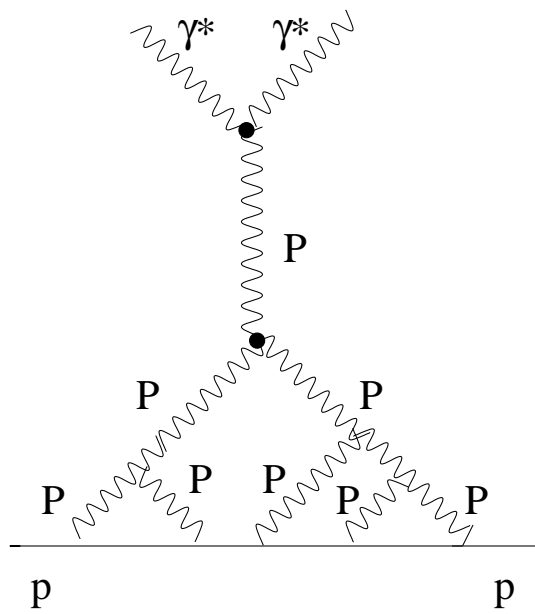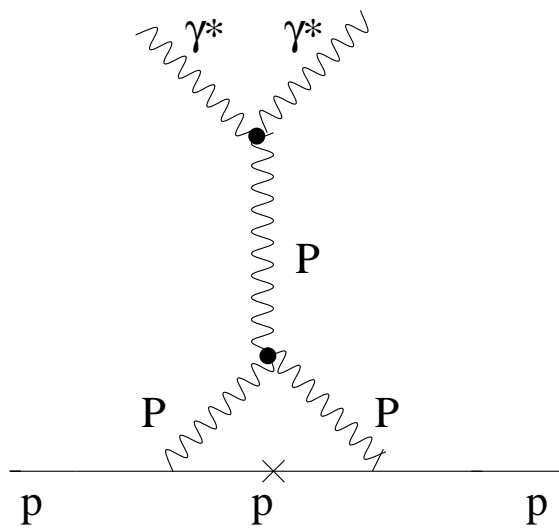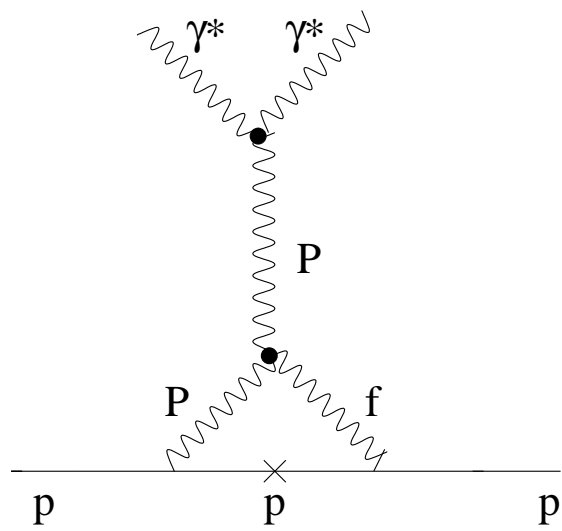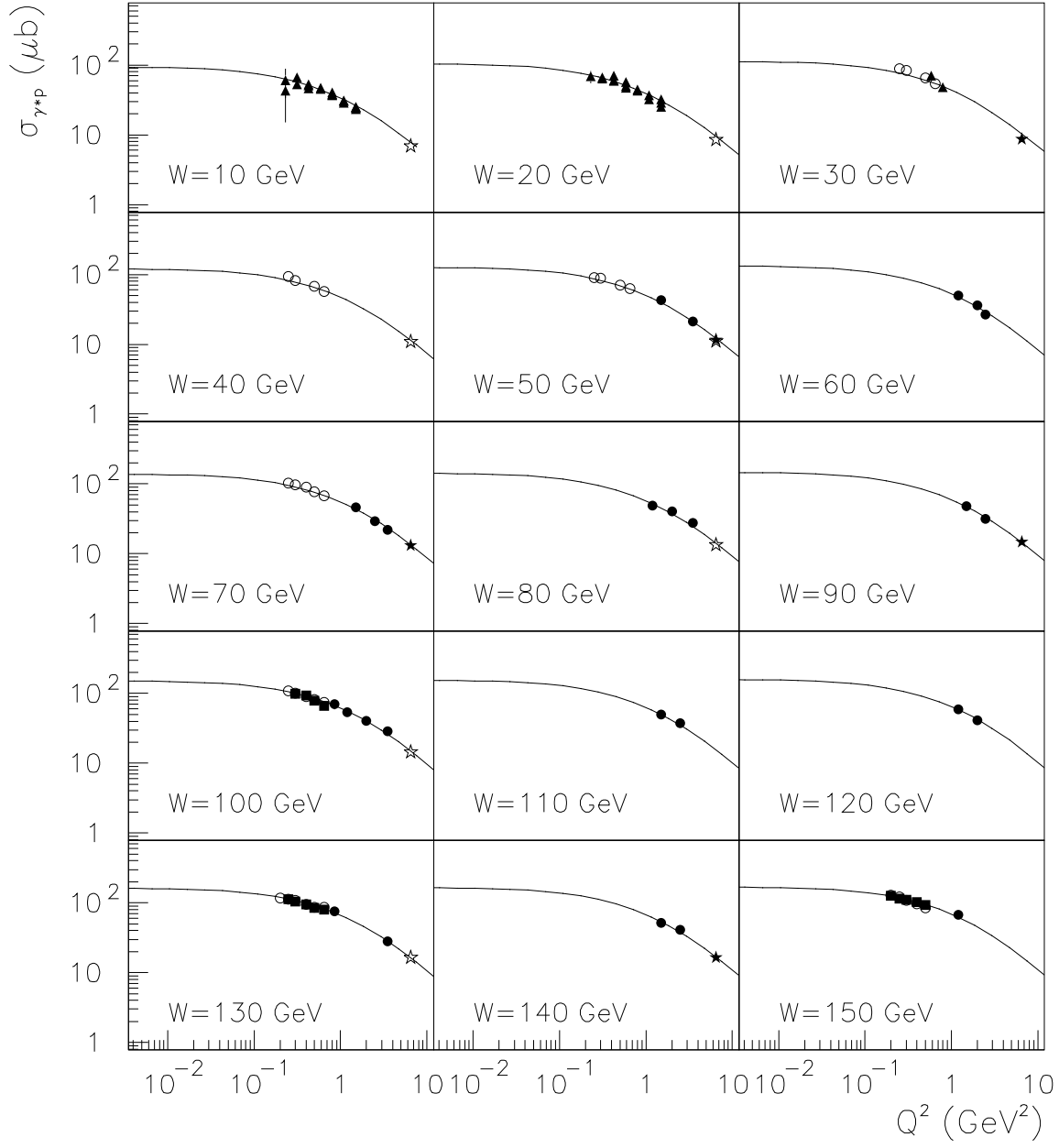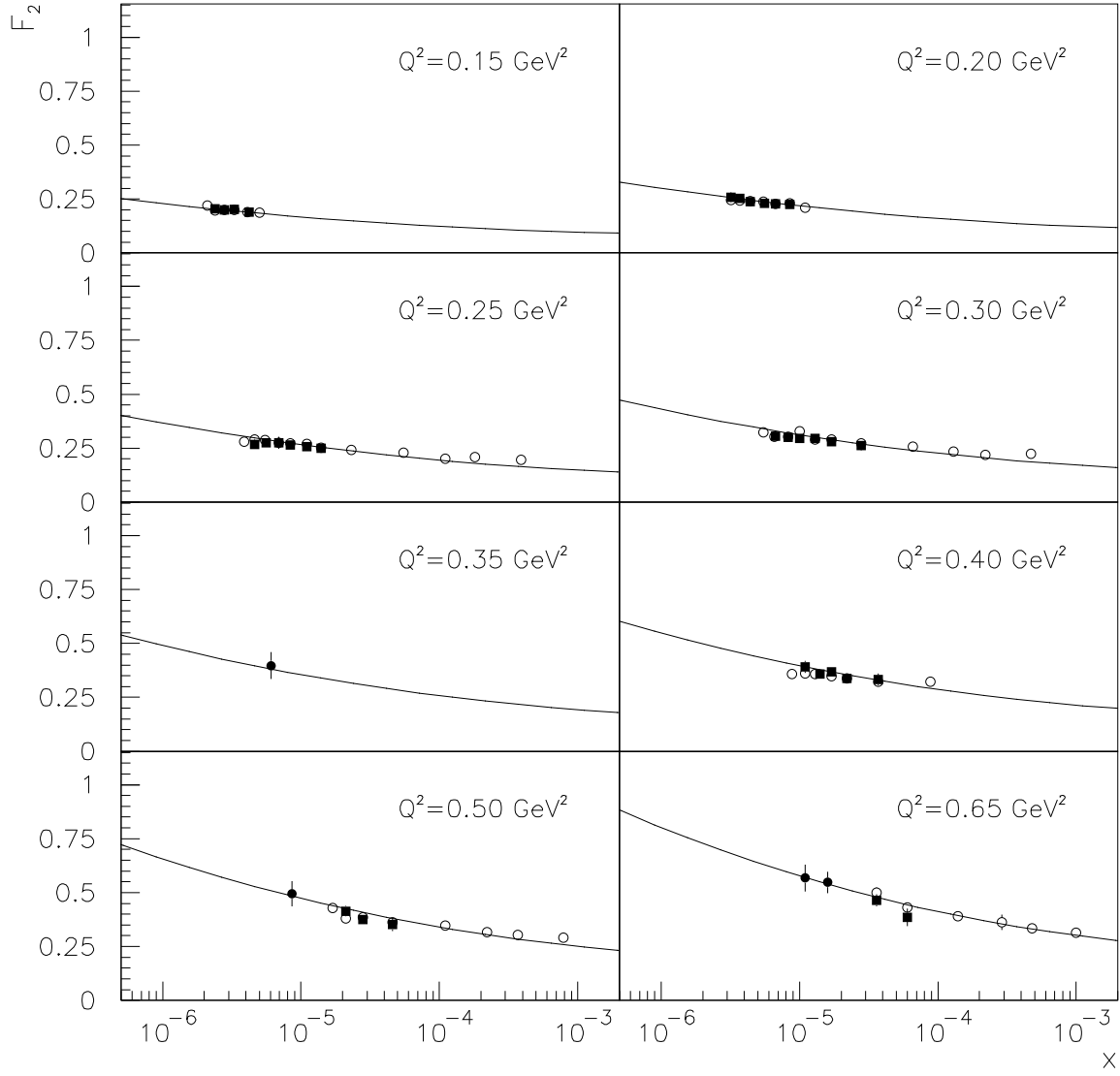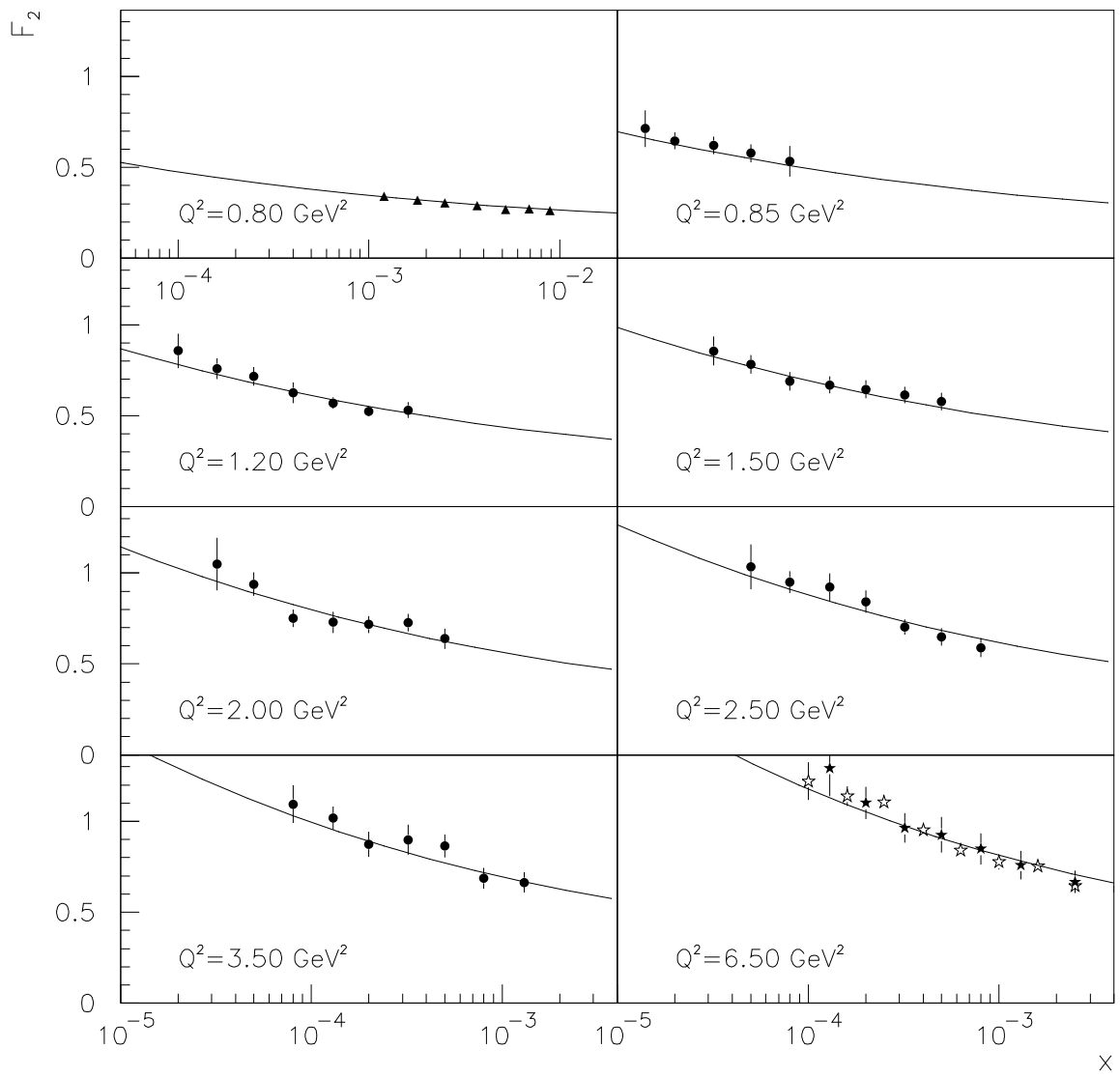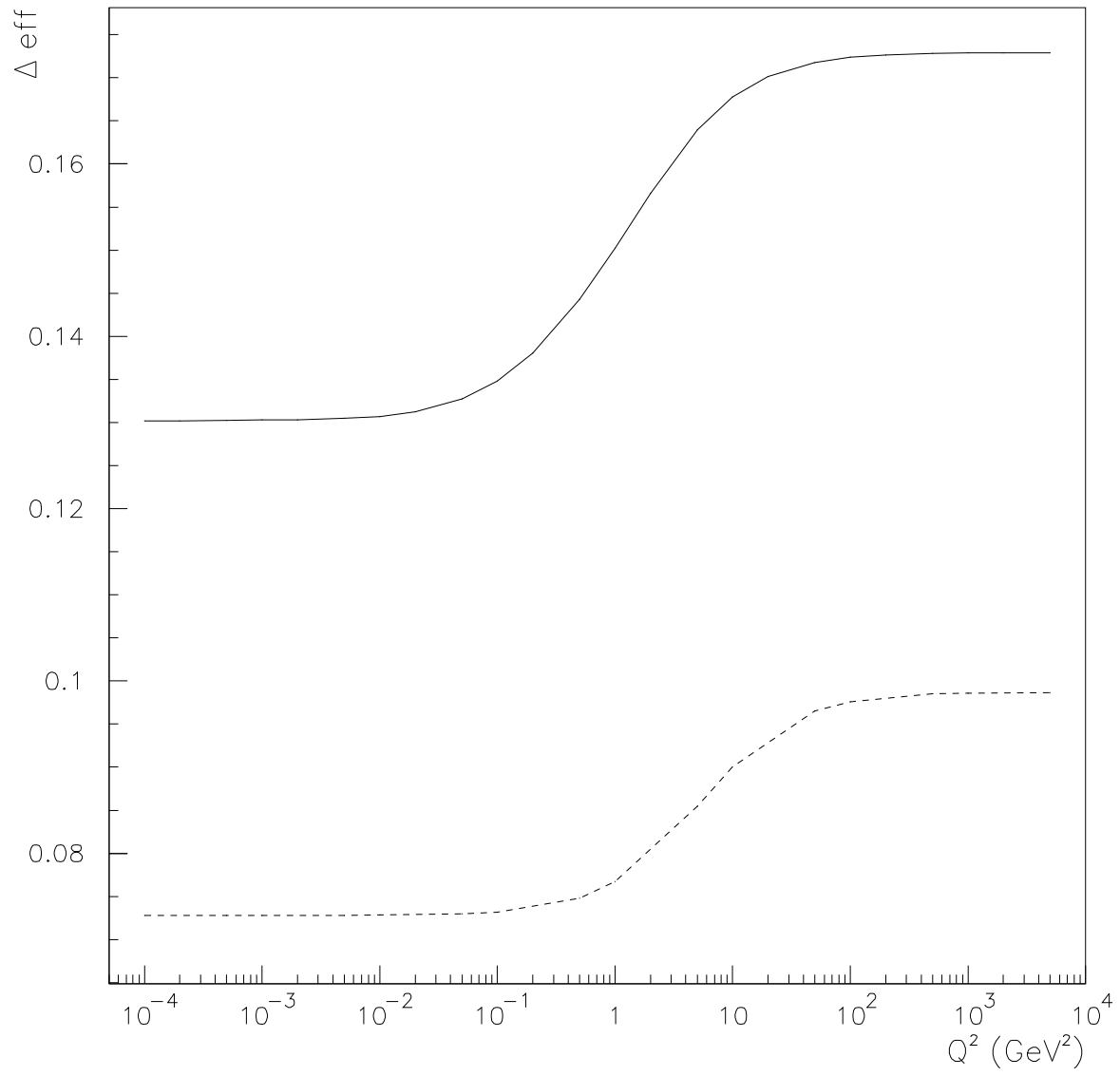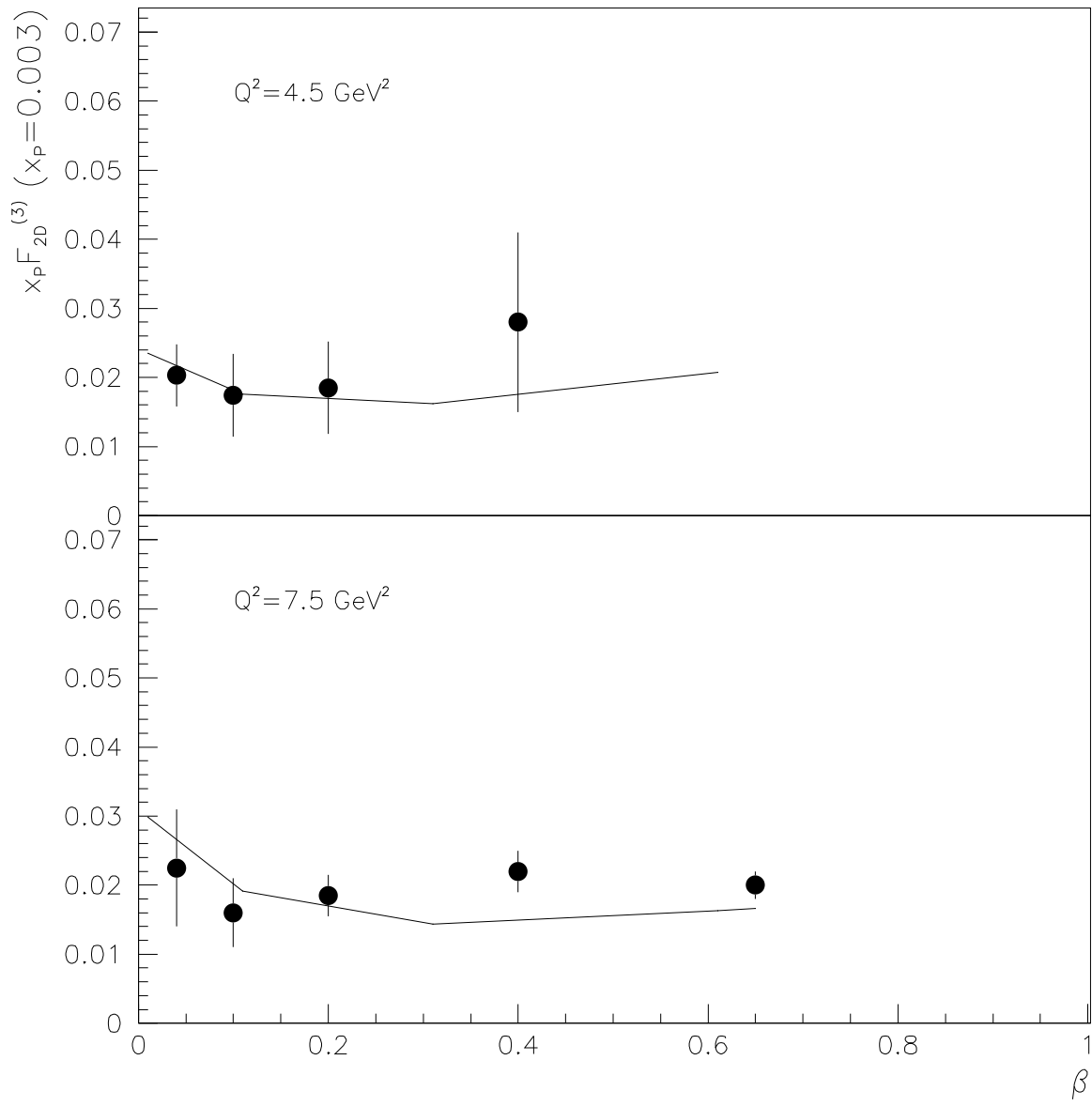
Figure 8

Figure 9

Figure 10

Figure 11

Figure 12

Figure 13